

Smooth, Efficient, and Interruptible Zooming and Panning

Andrew McCaleb Reach and Chris North

Abstract—This paper introduces a novel technique for smooth and efficient zooming and panning based on dynamical systems in hyperbolic space. Unlike the technique of van Wijk and Nuij, the animations produced by our technique are smooth at the endpoints and when interrupted by a change of target. To analyze the results of our technique, we introduce world/screen diagrams, a novel technique for visualizing zooming and panning animations.

1 INTRODUCTION

Zooming and panning is an interaction technique that solves the problem of fitting too-much data on a too-small screen. *Zooming* refers to the manipulation of scale—zooming in shows less in more detail, and zooming out shows more in less detail. *Panning* refers to the manipulation of the viewing window—panning left or right slides more information into view from one side of the screen, while information on the other side slides out of view.

In many user interfaces, the user zooms and pans manually by pinching a touch screen, rolling a scroll wheel, or by dragging the mouse. This paper does not focus on these problems—instead, this paper introduces techniques for *automatically* zooming and panning in response to user interactions.

For example, consider a home search application that shows homes matching the user’s query in two ways: in a list and on a map. A user who hovers the mouse over a home in the list will likely want to also see the home’s location on the map, and if this home is currently off-screen, this will require zooming and panning. If the user interface performs this navigation abruptly, jumping instantaneously from the old view to the new view, then the user loses all context about the spatial relationship between the current house and the previous house. By smoothly zooming and panning from one view to the next, the user gains a clearer understanding of the locations of the houses.

It can also be useful to combine manual zooming and automatic zooming. For example, imagine a stock price time series visualization in which the user manually zooms and pans on the time axis. As the user adjusts the time axis view, previously off-screen data will become visible, and some of this data may be outside the current range of the price axis. To prevent the user from having to manually readjust the price axis after zooming and panning on the time axis, it would be helpful for the interface to automatically zoom and pan on the price axis in order to continually accommodate the current range of prices.

The current state-of-the art technique for automatic zooming and panning is the smooth and efficient technique introduced by van Wijk and Nuij [18], which seeks to find a navigation animation that satisfies two properties:

1. The animation is *smooth* in the second order, i.e. both position and velocity are continuous.
2. The animation is *efficient*, i.e. it minimizes perceptual cost. For example, panning directly from a zoomed-in view of Seattle to a zoomed-in view of London is perceptually costly because the animation will require a long duration in order to avoid excessive motion blurring. By contrast, an animation that first zooms out from Seattle, then pans, then zooms into London is perceptually cheaper, since this animation can be made significantly shorter without excessive motion blurring.

• Andrew McCaleb Reach is with Virginia Tech. E-mail: caleb.reach@vt.edu.

• Chris North is with Virginia Tech. E-mail: north@cs.vt.edu.

The perceptual cost is quantified in terms of the *optical flow*, and a cost-minimizing zooming and panning animation is found via methods from differential geometry.

The animations produced by the technique of van Wijk and Nuij are smooth and efficient while in motion, but they technically violate the smoothness property at the beginning and end of the animation, where the velocity abruptly jumps from and to zero respectively. Moreover, if the animation is interrupted, then each interruption will, in general, introduce a velocity discontinuity. Prior research has shown preliminary evidence that animations without velocity discontinuities allow users to more easily track objects than animations with velocity discontinuities [7]. For the home-finding example, an interruption occurs every time the user hovers over a different home, and for the stock price example, interruptions occur continuously while the user zooms or pans. This renders the smooth and efficient zooming and panning technique unsuitable for situations in which animations are frequently interrupted by a change of target.

We solve the problem of smooth, efficient, and interruptible zooming and panning by applying ideas from the fields of signal processing and Riemannian geometry. Specifically, this paper makes the following contributions:

- We introduce the *hyperbolic model of zooming and panning*, in which a zoom and pan position is represented by a point in the Poincaré upper half-plane model of hyperbolic space. The hyperbolic model is a simplified version of u, w -space.
- Using this model, we show that smooth, efficient, and interruptible zooming and panning can be achieved by generalizing signal processing techniques to hyperbolic space.
- To visualize the results of our technique, we introduce *world/screen diagrams*, a novel method for visualizing zooming and panning trajectories that emphasizes the perceptual aspects of zooming and panning.

2 BACKGROUND

Zooming and panning is conceptually simple, but the details can be difficult to get right, and so several models have been proposed to aid in the understanding of zooming and panning. The space-scale diagrams of Furnas and Bederson [8] provide one way to represent zooming and panning. In this model, we imagine *world space* (i.e. the large information space that we are navigating) is projected from a stationary projector located at the origin. To zoom and pan, we maneuver a blank screen through the space-scale diagram. By bringing the blank screen closer to the projector, the projected image appears smaller on the screen, and so this motion corresponds to zooming out; and by moving the blank screen farther away from the projector, the projected image appears larger on the screen, and so this motion corresponds to zooming in. By moving the blank screen from side to side, different portions of the projected image will fall onto the screen, and so this motion corresponds to panning. A zooming and panning animation can be plotted as a screen-trajectory in a space-scale diagram, allowing zooming and panning animations to be visualized and compared.

Another model of zooming and panning is the u, w -space model of van Wijk and Nuij [18, 19]. In the u, w -space model, we imagine that

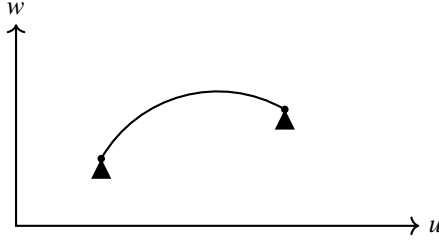


Fig. 1: In u, w space, a view is encoded by a point in two-dimensional space that represents the location of a camera. The u coordinate specifies the location in world space that is mapped to the center of screen space. The w coordinate specifies the width of the world-space span that is shown onscreen. A zooming and panning animation can be depicted as a path through u, w space, as shown.

world space is a stationary plane that is viewed through a camera. To zoom out, we move the camera away from the world plane, and to zoom in, we move the camera towards the world plane. To pan, we move the camera from side to side. In u, w -space, the location of the camera is represented by u , which gives the pan position, and w , which gives the zoom factor. Specifically, u is the world-space point that is mapped to the center of screen space, and w is the world-space length spanned by the width of the screen. The camera has an angle of view of approximately 53° . Additionally, in u, w -space, there is a *metric*, which approximates the perceptual cost of a zooming and panning animation. Using this metric, cost-minimizing animation paths were found by van Wijk and Nuij. This metric has a parameter ρ that controls the trade-off between zooming and panning, and when $\rho = 1$, this model is equivalent to hyperbolic geometry [19]. A diagram depicting u, w space is shown in Figure 1.

Like u, w -space, the model we use in this paper is based on a camera analogy and a perceptual cost metric. Unlike u, w -space, we do not assume that the camera has a specific angle of view, and in exchange, our perceptual cost metric is simpler without loss of generality. Specifically, our metric is always the metric for hyperbolic geometry, and the trade-off between zooming and panning is instead expressed by varying the camera's angle of view rather than by varying the metric.

This paper considers methods for automatically zooming and panning between views. There is much prior work on manual zooming and panning [9, 2, 5] where the user controls the zoom and pan positions directly. Prior work on automatic zooming and panning includes the speed-dependent automatic zooming technique of Igarashi and Hinckley [10], which automatically controls the zoom position in response to user-performed scrolling. Specifically, in the technique of Igarashi and Hinckley, the user controls the rate of scrolling, and the system automatically adjusts the zoom factor to accommodate the current scroll rate, i.e. the system zooms out as the scroll rate increases and zooms back in as the scroll rate decreases. A technique based on the u, w -space model has also been applied to this problem [19]. While ideas presented in this paper may have applications to the problem of speed-dependent automatic zooming, this paper will only focus on the problem of automatic zooming and panning between specified views.

3 ZOOMING AND PANNING REPRESENTATIONS

This section introduces a representation of zooming and panning in which each specific zooming and panning view is represented by the location of a camera. This model is the same as the u, w -space model of van Wijk and Nuij except for one aspect: we do not make any assumptions about the field of view of the camera. By not assuming a particular field of view, we simplify calculations in the following sections compared with u, w -space. We will consider both the case of zooming and panning over a two-dimensional space and the case of zooming and panning over a one-dimensional space.

For zooming and panning in a one-dimensional space, each zoom

and pan position can be described as a point $\mathbf{x} \in \mathbb{H}^2$ that represents the location of a camera, where the set \mathbb{H}^2 is defined by

$$\mathbb{H}^2 = \left\{ \begin{bmatrix} u \\ v \end{bmatrix} : u \in \mathbb{R}, v \in \mathbb{R}_{>0} \right\}$$

We can decompose a camera position $\mathbf{x} \in \mathbb{H}^2$ into two parts as follows:

$$\mathbf{x} = \begin{bmatrix} u \\ v \end{bmatrix}$$

We will refer to the u component as the *footprint* of the camera, and to the v component as the *altitude* of the camera. The camera points straight down at the u axis, and whichever portion of the u axis is captured by the camera is the portion of world-space that is shown onscreen.

For zooming and panning in two dimensions, each zoom and pan position can be represented as a point $\mathbf{x} \in \mathbb{H}^3$ that gives the location of a camera in three-dimensional space, where the set \mathbb{H}^3 is defined by

$$\mathbb{H}^3 = \left\{ \begin{bmatrix} \mathbf{u} \\ v \end{bmatrix} : \mathbf{u} \in \mathbb{R}^2, v \in \mathbb{R}_{>0} \right\}$$

As before, we will decompose this point into two parts:

$$\mathbf{x} = \begin{bmatrix} \mathbf{u} \\ v \end{bmatrix} = \begin{bmatrix} u_1 \\ u_2 \\ v \end{bmatrix}$$

where \mathbf{u} is the footprint and v is the altitude. This camera points down at the $v = 0$ plane.

To avoid needless repetition, we will describe our solution in a manner that applies at once to both the one-dimensional and two-dimensional cases. We will use \mathbb{H}^n to denote the set of zooming and panning positions, where $n = 2$ for one-dimensional zooming and panning and $n = 3$ for two-dimensional zooming and panning. The camera location is therefore a point $\mathbf{x} \in \mathbb{H}^n$, and the footprint $\mathbf{u} \in \mathbb{R}^{n-1}$ is then either a one-dimensional vector or a two-dimensional vector.

The relationship between a world-space point $\mathbf{p} \in \mathbb{R}^n$ and the corresponding screen-space point $\mathbf{r} \in \mathbb{R}^n$ is given by

$$\mathbf{p} = v\mathbf{r} + \mathbf{u} \quad (1)$$

This can, of course, be written in inverse form as

$$\mathbf{r} = \frac{\mathbf{p} - \mathbf{u}}{v}$$

which better reflects the more common operation in visualization of mapping from world space to screen space¹.

The specific cropping of screen space defines the field of view of the camera. For a 90° camera, screen space is the interval $[-1, 1]$ when $n = 1$ and the square region $[-1, 1] \times [-1, 1]$ when $n = 2$.

4 THE PERCEPTUAL COST METRIC

In this section, we will now introduce a *metric*, i.e. a way to quantify distance. Our metric will define distance in the space of zooming and panning positions to be an approximation of perceptual cost.

We will quantify the perceptual cost ds incurred by a small change $d\mathbf{x}$ in camera position by

$$ds = \frac{\|d\mathbf{x}\|}{v}. \quad (2)$$

where $\|d\mathbf{x}\|$ is the Euclidean norm of $d\mathbf{x}$ and v is the altitude of the camera position \mathbf{x} . In other words, perceptual cost is proportional to the Euclidean distance that the camera moves (which includes both changes

¹The choice of having a simpler mapping from screen space to world space than the other way around may seem odd, but it is the price paid for the camera analogy, and, more importantly, this choice simplifies later equations.

in footprint and altitude), and inversely proportional to the camera's altitude. Notice that unlike Euclidean space, in which distance depends only on the displacement vector, the metric we have introduced depends on both the camera's displacement vector $d\mathbf{x}$ and on the camera's altitude v .

The set \mathbb{H}^n together with (2) is the Poincaré upper half-space model of hyperbolic space, which has been widely studied in the field of Riemannian geometry. We will therefore frequently refer to camera positions as points in hyperbolic space.

This choice of metric can be explained intuitively. Imagine a camera with a 90° field of view. For an altitude of one meter, panning by half of the screen will require a movement of one meter. For an altitude of two meters, panning half the screen will require a movement of two meters. For an altitude of three meters, panning half the screen will require a movement of three meters. Clearly then, the onscreen effect of panning depends on both the distance that the camera moves and the altitude of the camera. For a given altitude, moving the camera a greater distance will, of course, result in a greater onscreen movement: therefore perceptual cost should be proportional to the distance the camera moves. However, since a proportionally larger distance is required for the same perceptual cost at higher altitudes, the perceptual cost of panning should be inversely related to altitude.

Now consider zooming. At an altitude of one meter, the camera must move upwards (i.e. in the direction of increasing altitude) by one meter to zoom out by a factor of two. We assume that zooming out by a constant factor will have the same perceptual cost regardless of where the camera is located. At an altitude of two meters, the camera must move upwards by two meters to zoom out by a factor of two. At an altitude of three meters, the camera must move upwards by three meters to zoom out by a factor of two. Therefore, like panning, the perceptual cost of zooming depends on both the distance traveled and the altitude, and like panning, the cost of zooming should be proportional to the distance zoomed and inversely proportional to altitude².

The perceptual cost of panning is related to the camera's angle of view—the distance required to pan one screen for a camera with a narrow angle of view is much smaller than that required to pan one screen for a camera with a wide angle of view. The perceptual cost of zooming, however, is not related to the camera's angle of view—zooming out by a factor of two requires the same camera movement regardless of the angle of view. Therefore, by varying the camera's angle of view, different trade-offs can be made between zooming and panning. A narrow angle of view expresses a preference for panning rather than zooming, and a wide angle of view expresses a preference for zooming rather than panning.

4.1 Comparison with u, w -space

In the u, w -space model, the camera's field of view is fixed, and a parameter ρ that appears in the metric controls the trade-off between zooming and panning. By contrast, in the hyperbolic model, the metric has no parameter to control the trade-off between zooming and panning—instead the camera has a variable field of view. By increasing the field of view, the same trajectory appears to zoom more and pan less, and by decreasing the field of view, the trajectory appears to pan more and zoom less. This is because the same onscreen view will map to different camera locations depending on the angle of view—a camera with a narrow angle of view will need to be located at a higher altitude to capture the same image as camera with a wide angle of view. In Smooth and Efficient Zooming and Panning [18], a user study found that the user-preferred value of ρ was 1.42, which is roughly $\sqrt{2}$. Interestingly, for $\rho = \sqrt{2}$ in the u, w -space model, the corresponding

²It might seem as though the relationship between camera distance and the perceptual cost of zooming is more complicated than this, since we would expect zooming out by a factor of two to have the same perceptual cost as zooming in by a factor of two, but at an altitude of two meters a two-meter movement is required to zoom out by a factor of two, whereas only a one-meter movement is required to zoom in by a factor of two. However, this discrepancy becomes smaller with shorter movements of the camera, and since the metric quantifies the effect of an infinitesimal movement of the camera, this discrepancy disappears.

angle of view in the hyperbolic model is exactly 90°, as is shown later in this section.

Our model has the following advantages over u, w -space:

1. The hyperbolic model of zooming and panning is precisely the same as the Poincaré upper half-space model of hyperbolic space, which has been well-studied in Riemannian geometry. Therefore, a large body of work in differential geometry on the half-space model immediately applies to zooming and panning.
2. In u, w -space, the parameter ρ appears in many of the equations that define the optimal zooming and panning trajectory. These equations are simpler in the hyperbolic model.
3. In the coordinates of u, w -space, the optimal path is an elliptical trajectory, where the eccentricity of the ellipse is determined by the parameter ρ . As we will see, in the coordinates of the hyperbolic model, the optimal path is always a simpler circular path.
4. In u, w -space, the w parameter is less intuitive if the screen is not square, since it gives the length of only one of the screen's sides, and the other must be calculated from the screen's aspect ratio. By contrast, in the hyperbolic model, we simple use two angles of view instead of one.

The hyperbolic model and u, w -space are related by a change of coordinates. Under this change of coordinates, the models are *equivalent up to scaling*, by which we mean that the optimal paths are the same with respect to this change of coordinates and the distances between points are related by a constant factor. We will now describe more precisely what it means for two models to be equivalent up to scaling. One way to interpret the condition of equivalence up to scaling is that the two models agree in every way except that distances are calculated in different units, e.g. one model might give the distance in inches whereas the other model gives the distance in centimeters. In practice this difference is unimportant, since even if a parameter was added to scale the metric by an arbitrary factor, this parameter would be redundant with other existing parameters that control how the optimal path is used. For example, in the model of van Wijk and Nuij, there is a parameter V that controls how quickly the optimal path is traversed. If the metric is scaled by a factor of two, and so all points are twice as far away from each other, then an animation that matches the original can be produced by similarly scaling V by a factor of two, therefore traversing the path at twice the speed and reaching the destination at the same time as traversing the original path at the original speed. Therefore, when we say that two models are equivalent up to scaling, we mean that they are equivalent in all useful ways.

Specifically, the hyperbolic model is equivalent up to scaling to the u, w -space model using the change of coordinates³

$$w = \rho^2 v.$$

Hyperbolic distance s is related to u, w -space distance σ by

$$s = \rho^2 \sigma.$$

The angle of view θ in the hyperbolic model is related to ρ in u, w -space by the equation

$$\theta = 2 \arctan \frac{\rho^2}{2}.$$

As mentioned earlier, for $\rho = \sqrt{2}$, as was preferred by users in the study of van Wijk and Nuij [18], the above equation gives $\theta = 90^\circ$.

In the appendix to Smooth and Efficient Zooming and Panning [18], an embedding of u, w -space in three-dimensional space is shown. In hyperbolic geometry, the well-known *pseudosphere* gives such an

³In the case of $\rho = \sqrt{2}$, which was the user-preferred value as found by van Wijk and Nuij, this formula becomes $w = 2v$, which is easily remembered since the character w visually appears to be the concatenation of two v characters.

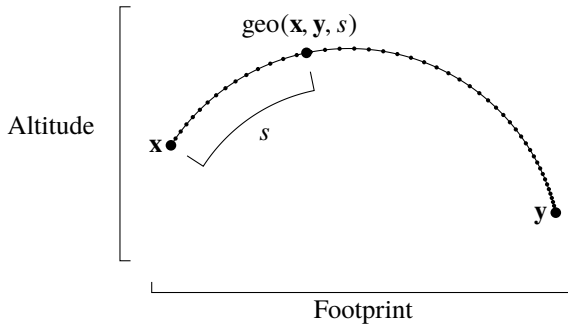


Fig. 2: The function $\text{geo}(\mathbf{x}, \mathbf{y}, s)$ returns the point arrived at by traveling from \mathbf{x} along a geodesic to \mathbf{y} for a hyperbolic distance s .

embedding, and can be written in terms of the footprint u and altitude v as:

$$\begin{aligned} x &= (\cos u)/v \\ y &= (\sin u)/v \\ z &= \operatorname{acosh} v - \tanh(\operatorname{acosh} v). \end{aligned}$$

Here \tanh denotes the hyperbolic tangent and acosh denotes the inverse hyperbolic cosine. It should be noted that, like the embedding of van Wijk and Nuij, this is only a *partial* embedding—in particular, it does not work for $v < 1$, since $\operatorname{acosh} v$ is imaginary for $v < 1$. Moreover, this mapping is ambiguous, since a point (x, y, z) corresponds to multiple values of u .

5 HYPERBOLIC SPACE

In this section we will explore the properties of hyperbolic space and how they relate to zooming and panning. First, we will discuss the geodesics of hyperbolic space, which correspond to perceptually optimal zooming and panning paths. Second, we will discuss vectors in hyperbolic space and operations that relate vectors and geodesics. We will use the properties and operations from this section later in this paper to develop algorithms for smooth, efficient, and interruptible zooming and panning.

We begin by exploring the geodesics of hyperbolic space. It is known that every geodesic in the Poincaré upper half-plane model is either a half-circle whose endpoints lie at altitude zero or a vertical line [4].

5.1 Geodesics and distance

We will define the function

$$\text{geo}(\mathbf{x}, \mathbf{y})$$

to be optimal path between $\mathbf{x} \in \mathbb{H}^n$ and $\mathbf{y} \in \mathbb{H}^n$, parameterized by arc length s as measured by the hyperbolic metric (2).

We will also define the function

$$\text{dist}(\mathbf{x}, \mathbf{y})$$

to be the hyperbolic distance between two camera locations; i.e. the perceptual cost of the optimal path between these two points. This function is the hyperbolic analog of Euclidean distance. We have the identities

$$\begin{aligned} \text{geo}(\mathbf{x}, \mathbf{y}, 0) &= \mathbf{x} \\ \text{geo}(\mathbf{x}, \mathbf{y}, \text{dist}(\mathbf{x}, \mathbf{y})) &= \mathbf{y} \\ \text{dist}(\mathbf{x}, \text{geo}(\mathbf{x}, \mathbf{y}, s)) &= s \end{aligned}$$

The function geo is depicted in Figure 2.

Finally, we will define a third function, gerp , in terms of geo and dist as

$$\text{gerp}(\mathbf{x}, \mathbf{y}, \alpha) = \text{geo}(\mathbf{x}, \mathbf{y}, \alpha \text{dist}(\mathbf{x}, \mathbf{y})) \quad (3)$$

This function interpolates between \mathbf{x} at $\alpha = 0$ and \mathbf{y} at $\alpha = 1$ along a perceptually optimal path.

The functions geo and dist can be calculated as

$$\text{dist}\left(\left[\begin{smallmatrix} \mathbf{u}_0 \\ v_0 \end{smallmatrix}\right], \left[\begin{smallmatrix} \mathbf{u}_1 \\ v_1 \end{smallmatrix}\right]\right) = S \quad (4a)$$

$$\text{geo}\left(\left[\begin{smallmatrix} \mathbf{u}_0 \\ v_0 \end{smallmatrix}\right], \left[\begin{smallmatrix} \mathbf{u}_1 \\ v_1 \end{smallmatrix}\right], s\right) = \left[\begin{smallmatrix} \mathbf{u}(s) \\ v(s) \end{smallmatrix}\right] \quad (4b)$$

where, for $\mathbf{u}_0 \neq \mathbf{u}_1$,

$$\mathbf{u}(s) = \mathbf{u}_0 + v_0 \frac{\sinh(s)}{\cosh(s + r_0)} \frac{\mathbf{u}_1 - \mathbf{u}_0}{\|\mathbf{u}_1 - \mathbf{u}_0\|} \quad (4c)$$

$$v(s) = v_0 \frac{\cosh(r_0)}{\cosh(s + r_0)} \quad (4d)$$

$$S = r_1 - r_0 \quad (4e)$$

$$r_i = \operatorname{asinh} \frac{v_i^2 - v_0^2 + (-1)^i \|\mathbf{u}_1 - \mathbf{u}_0\|^2}{-2v_i \|\mathbf{u}_1 - \mathbf{u}_0\|} \quad (4f)$$

and, for $\mathbf{u}_0 = \mathbf{u}_1$,

$$\mathbf{u}(s) = \mathbf{u}_0 \quad (4g)$$

$$v(s) = v_0 e^{sk} \quad (4h)$$

$$k = \operatorname{sign}(v_1 - v_0) \quad (4i)$$

$$S = |\log(v_1/v_0)|. \quad (4j)$$

In these equations, \sinh and \cosh denote the hyperbolic sine and cosine functions respectively, and asinh denotes the inverse hyperbolic sine. The notation sign denotes the sign function, which returns -1 when its argument is negative, 0 when its argument is zero, and 1 when its argument is positive. Finally, the notation \log is used to denote the natural logarithm. These equations were adapted from those given by van Wijk and Nuij [18], but were reformulated to decrease numerical error by removing sums and differences that caused catastrophic cancellation. Figure 7 visualizes the path produced by the function $\text{geo}(\mathbf{x}, \mathbf{y}, s)$ between two views \mathbf{x} and \mathbf{y} as a world/screen diagram.

5.2 Vectors in hyperbolic space

The functions defined in the last subsection operated on points in hyperbolic space. In the following subsections, we will define functions that manipulate both points and *vectors* in hyperbolic space. In the same way that a point in hyperbolic space can be used to represent the *position* of a camera, a vector in hyperbolic space can be used to represent the *velocity* of a camera. In this subsection we will introduce a notion of vectors in hyperbolic space. These ideas can be found in most textbooks on differential and Riemannian geometry [6, 12, 11].

In Euclidean space, a vector has a direction and a magnitude. In Riemannian geometry, a vector additionally has a point at which it's based. This is necessary because the fundamental properties of the space change depending on where the base point is located. We will use bold capital letters, e.g. \mathbf{X} , to denote vectors in hyperbolic space, and we will use the notation $\mathbb{T}_{\mathbf{x}}\mathbb{H}^n$ to denote the set of all vectors located at point \mathbf{x} .

The hyperbolic magnitude $|\mathbf{X}|$ of a vector $\mathbf{X} \in \mathbb{T}_{\mathbf{x}}\mathbb{H}^n$ is defined as

$$|\mathbf{X}| = \frac{\|\mathbf{X}\|}{v}$$

where $\|\mathbf{X}\|$ is the Euclidean norm of \mathbf{X} , and v is the altitude of \mathbf{x} . This definition mirrors the definition of the metric. This must be the case because the magnitude of a velocity vector must give a notion of speed, i.e. the rate of change of distance, and this notion must match the notion of length defined by the metric.

5.3 Exponential map

We will now define a function, the *exponential map*, that takes a vector in hyperbolic space as input. The exponential map $\text{Exp}(\mathbf{X})$ of the vector $\mathbf{X} \in \mathbb{T}_{\mathbf{x}}\mathbb{H}^n$ gives the point arrived at by traveling a hyperbolic distance

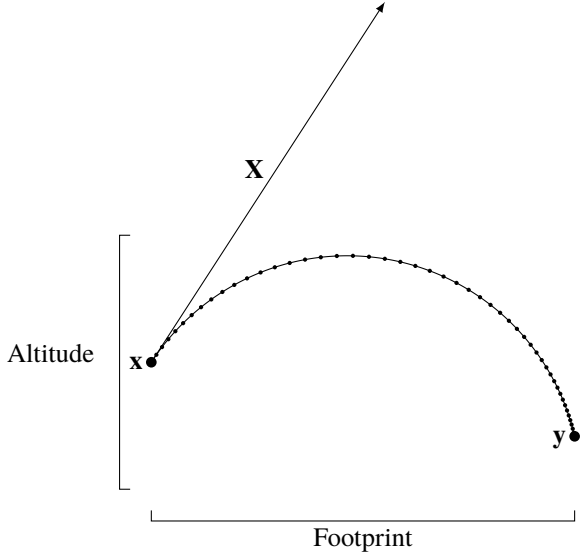


Fig. 3: The hyperbolic exponential map $\text{Exp}(\mathbf{X})$ sends a vector $\mathbf{X} \in \mathbb{T}_x\mathbb{H}^n$ to the point $\mathbf{y} = \text{Exp}(\mathbf{X})$ by finding a geodesic $\gamma(t)$ whose initial velocity $\gamma'(0)$ is equal to \mathbf{X} and then calculating $\mathbf{y} = \gamma(1)$. The hyperbolic logarithmic map $\text{Log}_x(\mathbf{y})$, by contrast, sends two points \mathbf{x} and \mathbf{y} to the vector $\mathbf{X} = \text{Log}_x(\mathbf{y})$ by finding a geodesic $\gamma(t)$ whose endpoints are $\gamma(0) = \mathbf{x}$ and $\gamma(1) = \mathbf{y}$ and then calculating $\mathbf{X} = \gamma'(0)$, where $\gamma'(0)$ is the initial velocity of $\gamma(t)$. The exponential and logarithmic maps are therefore inverses of each other.

$|\mathbf{X}|$ from \mathbf{x} along an optimal path with initial direction matching \mathbf{X} . This process is depicted in Figure 3.

For a vector $\mathbf{X} \in \mathbb{T}_x\mathbb{H}^n$ with footprint and altitude components \mathbf{U} and V respectively located at the base point \mathbf{x} with footprint \mathbf{u}_0 and altitude v_0 , the exponential map can be calculated as

$$\text{Exp}(\mathbf{X}) = \begin{bmatrix} \mathbf{u}_1 \\ v_1 \end{bmatrix} \quad (5a)$$

where, for $\mathbf{U} \neq 0$,

$$\mathbf{u}_1 = \mathbf{u}_0 + \frac{v_0 \sinh |\mathbf{X}|}{\cosh(|\mathbf{X}| + r_0)} \frac{\mathbf{U}}{\|\mathbf{U}\|} \quad (5b)$$

$$v_1 = v_0 \frac{\cosh(r_0)}{\cosh(|\mathbf{X}| + r_0)} \quad (5c)$$

$$r_0 = -\operatorname{asinh} \frac{V}{\|\mathbf{U}\|}. \quad (5d)$$

and, for $u_0 = u_1$,

$$U = 0 \quad (5e)$$

$$W = v_0 \log(v_1/v_0) \quad (5f)$$

5.4 Logarithmic map

The logarithmic map takes two points $\mathbf{x}, \mathbf{y} \in \mathbb{H}^n$ as arguments and produces a vector $\text{Log}_x(\mathbf{y})$ that points in the direction of \mathbf{y} along an optimal path from \mathbf{x} , where the magnitude of this vector is equal to $\text{dist}(\mathbf{x}, \mathbf{y})$. The logarithmic map can be defined by

$$\text{Log}_x(\mathbf{y}) = \text{gerp}'(\mathbf{x}, \mathbf{y}, 0)$$

where gerp' denotes the derivative of gerp with respect to its last parameter. Then $\text{Log}_x(\mathbf{y}) \in \mathbb{T}_x\mathbb{H}^n$ is the initial velocity in hyperbolic space of the optimal path from \mathbf{x} at $t = 0$ to \mathbf{y} at $t = 1$, and so this operation is analogous to the subtraction $\mathbf{y} - \mathbf{x}$ in Euclidean space.

Calculations reveal that for $\mathbf{x}_0, \mathbf{x}_1 \in \mathbb{H}^n$ with respective footprints $\mathbf{u}_0, \mathbf{u}_1$ and altitudes v_0, v_1 , the logarithmic map is given by

$$\text{Log}_{\mathbf{x}_0}(\mathbf{x}_1) = \mathbf{X} \quad (6a)$$

where, for $\mathbf{u}_0 \neq \mathbf{u}_1$, the footprint \mathbf{U} and altitude V components of \mathbf{X} are given by

$$U = v_0 S \operatorname{sech}(r_0) \frac{\mathbf{u}_1 - \mathbf{u}_0}{\|\mathbf{u}_1 - \mathbf{u}_0\|} \quad (6b)$$

$$W = -v_0 S \tanh r_0 \quad (6c)$$

$$S = r_1 - r_0 \quad (6d)$$

$$r_i = \operatorname{asinh} \frac{v_1^2 - v_0^2 + (-1)^i \|\mathbf{u}_1 - \mathbf{u}_0\|^2}{-2v_i \|\mathbf{u}_1 - \mathbf{u}_0\|} \quad (6e)$$

If $\mathbf{u}_0 = \mathbf{u}_1$, then (\mathbf{U}, W) is given by

$$U = 0 \quad (6f)$$

$$W = v_0 \log(v_1/v_0) \quad (6g)$$

The exponential and logarithmic maps are inverses of each other, i.e.

$$\text{Exp}(\text{Log}_x(\mathbf{y})) = \mathbf{y}.$$

A useful identity that we will use later relating the exponential map, logarithmic map, and geodesic interpolation is

$$\text{Exp}(t \text{Log}_x(\mathbf{y})) = \text{gerp}(\mathbf{x}, \mathbf{y}, t) \quad (7)$$

5.5 Covariant derivative

In Euclidean space, we can calculate acceleration by differentiating velocity. However, the second derivative of $\text{gerp}(\mathbf{x}, \mathbf{y}, t)$ will generally be nonzero, since geodesics in hyperbolic geometry are generally curved. However, geodesics are the hyperbolic analog of straight lines in Euclidean space, and so it's reasonable to desire a hyperbolic analog of acceleration for which geodesics have zero hyperbolic acceleration.

In Riemannian geometry, this notion is provided by the *covariant derivative*, which provides a way to differentiate time-varying vectors. Hyperbolic acceleration is then given by the covariant derivative of velocity. The covariant derivative can be defined in terms of the metric [6], and calculations reveal that the covariant derivative for hyperbolic space is given by

$$\frac{D\mathbf{X}}{dt} = \mathbf{X}' \quad (8a)$$

where the footprint \mathbf{U}' and altitude V' components of \mathbf{X}' are given by

$$\mathbf{U}' = \frac{d\mathbf{U}}{dt} - \frac{1}{v} \left(\frac{dv}{dt} \mathbf{U} + \frac{d\mathbf{u}}{dt} V \right) \quad (8b)$$

$$V' = \frac{dV}{dt} + \frac{1}{v} \left(\frac{d\mathbf{u}}{dt} \cdot \mathbf{U} - \frac{dv}{dt} V \right) \quad (8c)$$

in which \mathbf{u} and v are the footprint and altitude of \mathbf{x} , the base point of \mathbf{X} .

5.6 Transport map

In Euclidean space, vectors do not need to keep track of their base points, because a vector formed at one point can be easily used at any other point. For example, consider the expression $\mathbf{z} + (\mathbf{y} - \mathbf{x})$. In this expression, the subtraction $\mathbf{y} - \mathbf{x}$ is used to form a vector from base point \mathbf{x} pointing to \mathbf{y} , and then this vector is used in an operation with a different point \mathbf{z} . In hyperbolic space, things are not so simple. If we try to directly change the base of a vector, e.g. change $\mathbf{X} \in \mathbb{T}_x\mathbb{H}^n$ to $\mathbf{Y} \in \mathbb{T}_y\mathbb{H}^n$, then basic properties of the vector may change, e.g. the hyperbolic magnitude of these two vectors will not match if the altitude of \mathbf{x} does not equal the altitude of \mathbf{y} .

In Riemannian geometry, the *parallel transport* operation allows a vector to be moved to another location. The result of parallel transporting a vector depends not just on the end points and the vector, but also on the specific path taken. We will now define a *transport map*, which moves vectors to another location along a geodesic.

For points $\mathbf{x}_0, \mathbf{x}_1$ with respective footprints $\mathbf{u}_0, \mathbf{u}_1$ and altitudes v_0, v_1 , the transport map of a vector $\mathbf{X} \in \mathbb{T}_{\mathbf{x}_0}\mathbb{H}^n$ to \mathbf{x}_1 is given by

$$\mathcal{T}_{\mathbf{x}_1}(\mathbf{X}) = \begin{bmatrix} \mathbf{U}_1 \\ V_1 \end{bmatrix} \quad (9a)$$

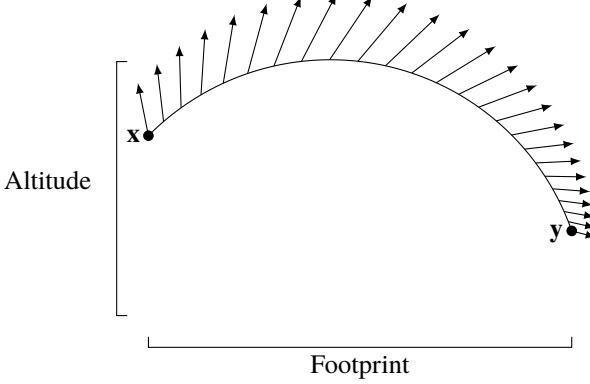


Fig. 4: The transport map $T_y(\mathbf{X})$ of the hyperbolic vector $\mathbf{X} \in \mathbb{H}^n$ is the vector $\mathbf{Y} \in \mathbb{H}^n$ obtained by parallel transporting \mathbf{X} to the new base point $y \in \mathbb{H}^n$ along a geodesic from x to y . In hyperbolic space, the transport map causes the Euclidean magnitude to change so that the hyperbolic magnitude remains the same—if the target altitude is higher than the starting altitude, then the Euclidean magnitude will grow, and if the target magnitude is lower than the starting altitude, then the Euclidean magnitude will shrink. The vector will also rotate, keeping a constant Euclidean angle with the geodesic.

where, for $\mathbf{u}_0 \neq \mathbf{u}_1$,

$$\mathbf{U}_1 = \frac{v_1}{v_0} \mathbf{U}_0^\perp + \frac{v_1}{v_0} \operatorname{Re}(z_1) \frac{\mathbf{u}_1 - \mathbf{u}_0}{\|\mathbf{u}_1 - \mathbf{u}_0\|} \quad (9b)$$

$$V_1 = \frac{v_1}{v_0} \operatorname{Im}(z_1) \quad (9c)$$

$$z_1 = \vartheta_1 \bar{\vartheta}_0 z_0 \quad (9d)$$

$$z_0 = U_0^\parallel + W_0 i \quad (9e)$$

$$U_0^\parallel = \mathbf{U}_0 \cdot \frac{\mathbf{u}_1 - \mathbf{u}_0}{\|\mathbf{u}_1 - \mathbf{u}_0\|} \quad (9f)$$

$$\mathbf{U}_0^\perp = \mathbf{U}_0 - U_0^\parallel \frac{\mathbf{u}_1 - \mathbf{u}_0}{\|\mathbf{u}_1 - \mathbf{u}_0\|} \quad (9g)$$

$$\vartheta_i = \tanh r_i + i \operatorname{sech} r_i \quad (9h)$$

$$r_i = \operatorname{asinh} \frac{v_1^2 - v_0^2 + (-1)^i \|\mathbf{u}_1 - \mathbf{u}_0\|^2}{-2v_i \|\mathbf{u}_1 - \mathbf{u}_0\|} \quad (9i)$$

and, for $\mathbf{u}_0 = \mathbf{u}_1$,

$$\mathbf{U}_1 = \frac{v_1}{v_0} \mathbf{U}_0 \quad (9j)$$

$$V_1 = \frac{v_1}{v_0} V_0 \quad (9k)$$

In these equations, i denotes the imaginary unit, and $\bar{\vartheta}_0$ denotes the complex conjugate of ϑ_0 . The functions Re and Im the real and imaginary parts of their respective arguments. Imaginary numbers are used in these equations to perform rotations. The result of the transport map is shown in Figure 4.

6 VISUALIZING ZOOMING AND PANNING ANIMATIONS

A simple way to visualize a zooming and panning path in \mathbb{H}^n is to simply plot the footprint on the x axis and the altitude on the y axis, i.e. simply plot the path the camera takes. This corresponds to the u, w -space diagrams of van Wijk and Nuij. However, it can be difficult to discern the perceptual effect of zooming and panning from these footprint/altitude diagrams.

To visualize a zooming and panning animation in a way that emphasizes the perceived motion, we introduce a novel visualization technique: *world/screen diagrams*. A world/screen diagram consists of

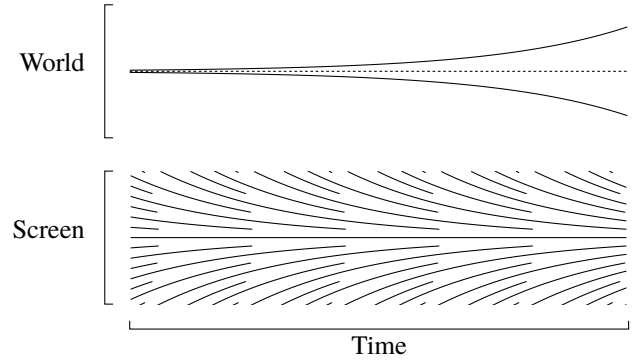


Fig. 5: A *world/screen diagram* for a zooming-out animation. The upper plot, the *screen bounds diagram*, shows the screen center and screen bounds plotted in world space over time. The lower plot, the *optical pathline diagram*, shows world points plotted in screen space over time. The slope of each line in the optical pathline diagram at each instant in time corresponds to the velocity of an onscreen point at that instant. As the animation progresses, the screen occupies an increasingly large portion of world-space, as can be seen in the screen bounds diagram. At the same time, a given portion of world space occupies an increasingly small portion screen space, as can be seen from the optical pathline diagram.

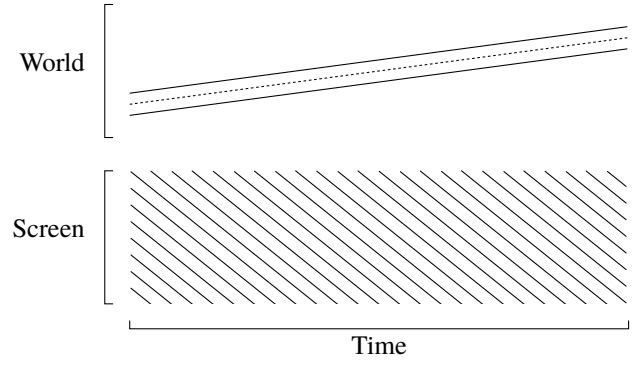


Fig. 6: A *world/screen diagram* for a panning animation. The world bounds diagram (above) shows that the screen moves through world space at a constant rate, and the optical pathline diagram (below) shows that world points move through screen space at a constant rate.

two sub-diagrams that share a common time axis. The upper part of the world/screen diagram is a *screen bounds diagram*, which plots the screen center and screen bounds in world space over time. The lower part of the world/screen diagram is an *optical pathline diagram*, which plots world points in screen space over time. An optical pathline diagram has time on the horizontal axis and screen space on the vertical axis, and each curve in the diagram is a constant point in world space. For each world-point curve in the optical pathline diagram, the slope of the curve corresponds to the onscreen velocity of the world point. Example world/screen diagrams are shown in Figures 5 to 7. By mapping time to a dedicated axis, the world/screen allows for precise visualizations of the temporal aspects of a zooming and panning animation. By contrast, in a u, w -space diagram, time must be encoded by color or by dots placed at regularly-spaced intervals in time.

One advantage of world/screen diagrams over other representations of zooming and panning trajectories is that the optical pathline diagrams corresponds more closely to the perception of zooming and panning than other diagrams. In fact, the root-mean-square optical flow velocity, which van Wijk and Nuij originally used to define their

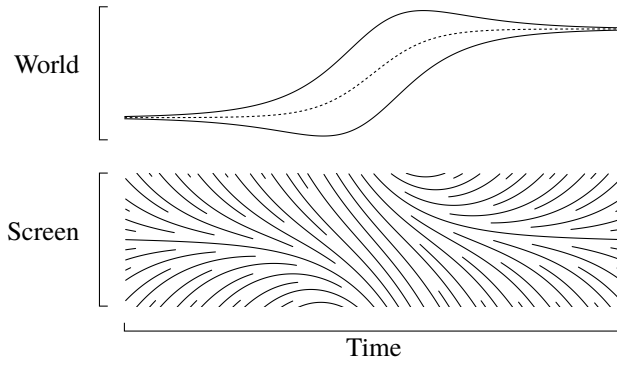


Fig. 7: A world/screen diagram for optimal zooming and panning. This diagram depicts zooming out, followed by panning, followed by zooming in. The specific zooming and panning path used was calculated using the smooth and efficient technique of van Wijk and Nuij.

metric, can be determined for each time instant in the world/screen diagram by finding the root-mean-square slope of all pathlines at that instant. By contrast, points taken from a perceptually uniform trajectory at equally-spaced moments in time will appear to be unevenly spaced if plotted in a footprint/altitude diagram or a space-scale diagram, and so these diagrams do not accurately represent perception.

6.1 Optical pathline diagrams

We will now describe the algorithm we used to create the optical pathline diagrams in this paper. In principle, an optical pathline diagram can be created by taking any set of world-space points and plotting their paths in an optical pathline diagram. However, this approach leads to diagrams in which curves are closely spacing in some regions widely spaced in others. To remedy this problem, we add and remove world-point curves from the diagram as space allows.

We will now show that the problem of adding and removing world-point curves can be seen as a problem of adding and removing isolines (i.e. contour lines) from a scalar field. Consider the scalar field φ that maps time t and screen point r to the corresponding world point $p = \varphi(t, r) = v(t)r + u(t)$. The isolines of this field are the world-point curves in the optical pathline diagram. Therefore, we must choose when to add and remove isolines from the diagram.

Note that if $\varphi(t, r)$ is linear, then the gradient magnitude $\|\nabla\varphi(t, r)\|$ is constant over all t and r . In this case, if we add isolines at equally-spaced world-points, then the isolines will also be equally spaced. The world-point spacing P and screen-space isoline spacing R are related by

$$P = R\|\nabla\varphi(t, r)\|$$

In practice, the function $\varphi(t, r)$ will not be linear, but provided that it is sufficiently smooth, the above relationship will approximately hold. This relationship provides the intuition behind the algorithm we will describe.

Let the set $C_\alpha \subset \mathbb{R}^2$, for parameter $\alpha > 0$ that controls the spacing, be the set of all points in the optical pathline diagram at which a contour should be drawn. We define C_α as the set of all (t, r) such that there exists a power of two not less than $\alpha\|\nabla\varphi(t, r)\|$ that divides $\varphi(t, r)$. Using the notation

$$\lceil x \rceil = 2^{\lceil \log_2(x) \rceil}$$

the definition of C_α can be written as

$$C_\alpha = \{(t \in \mathbb{R}, r \in \mathbb{R}) : \lceil \alpha\|\nabla\varphi(t, r)\| \rceil \text{ divides } \varphi(t, r)\}.$$

This can be seen as a discretized version of the dense isocontour imaging technique of Matvienko and Krüger [14].

Now that we have defined C_α , we will describe an algorithm for computing the optical pathline diagrams. The optical pathline diagram

will take as input the parameter α which controls the spacing of the pathlines, the footprint and altitude functions $u(t)$ and $v(t)$, and the screen-space bounds r_{low} and r_{high} .

Notice that

$$\begin{aligned} \|\nabla\varphi(t, r)\|^2 &= \left(\frac{\partial}{\partial t}p(t, r)\right)^2 + \left(\frac{\partial}{\partial r}p(t, r)\right)^2 \\ &= (rv'(t) + u'(t))^2 + (v(t))^2 \end{aligned}$$

where $v'(t)$ and $u'(t)$ are the derivatives of $v(t)$ and $u(t)$ respectively. Because

$$|v(t)| = \left| \frac{\partial}{\partial r}p(t, r) \right| \leq \|\nabla p(t, r)\|,$$

a necessary condition for $(t, r) \in C_\alpha$ is that $\lceil \alpha|v(t)| \rceil$ divides $p(t, r)$. Taking advantage of this necessary condition, we can use the following algorithm to find the optical pathline diagram:

- Let A be an empty hash map.
- For each time step i :
 - Calculate

$$\begin{aligned} P &= \lceil \alpha|v(t_i)| \rceil \\ p_{\text{low}} &= P \left\lceil \frac{v(t_i)r_{\text{low}} + u(t_i)}{P} \right\rceil \\ p_{\text{high}} &= P \left\lceil \frac{v(t_i)r_{\text{high}} + u(t_i)}{P} \right\rceil. \end{aligned}$$
 - For each p in $p_{\text{low}}, p_{\text{low}} + P, p_{\text{low}} + 2P, p_{\text{low}} + 3P, \dots, p_{\text{high}}$:
 - * Calculate

$$\psi = \|\nabla\varphi(t, r)\| = \sqrt{(v(t))^2 + (rv'(t_i) + u'(t_i))^2}$$
 - If the derivatives v' and u' are not available (e.g. because the zooming and panning animation is computed frame-by-frame rather than as a continuous path), then they can be approximated by finite differences.
 - * If $\lceil \alpha\psi \rceil$ does not divide p then continue to the next p .
 - * Otherwise, check to see if $A[p]$ exists.
 - If $A[p]$ does not exist, assign to $A[p]$ a list containing i as its sole element.
 - If $A[p]$ does exist, append i to the list $A[p]$.
 - For each key p in A :
 - For each i in $A[p]$:
 - * Calculate the screen-space point r corresponding to p using

$$r = \frac{p - u(t_i)}{v(t_i)}$$
 - * If i is the first element in $A[p]$, or if the previous element in $A[p]$ was not $i-1$, then begin a new pathline at (t_i, r) .
 - * Otherwise, add a new segment to the current pathline that connects to (t_i, r) .

7 THE PROBLEM OF INTERRUPTIONS

The previous sections have developed the hyperbolic model of zooming and panning. We will now use this model to solve the interruptible zooming and panning problem.

In the interruptible zooming and panning problem, we are given as input a *target signal* $\mathbf{x}(t)$ and we must compute as output a *smoothed signal* $\mathbf{y}(t)$. At each instant t , the target camera position is given by $\mathbf{x}(t) \in \mathbb{H}^n$, and the smoothed camera position $\mathbf{y}(t) \in \mathbb{H}^n$ must be computed. Importantly, the computation of the smoothed camera position $\mathbf{y}(t)$ must depend only on $\mathbf{x}(\tau)$ for all $\tau < t$. In other words, the transformation from the target signal to the smoothed signal must be *causal*—the smoothed camera position must be computed at each instant using only the past and present behavior of the input signal. This models the real-world usage of interruptible zooming and panning in user interfaces, where future user input is unknowable.

Before we introduce the signal-processing-based solutions that are the main focus of this paper, we first describe two simple techniques and analyze their disadvantages. These simpler techniques assume that the target signal is a step function, i.e. the target camera position changes abruptly at times t_1, t_2, t_3, \dots but is otherwise constant.

7.1 Constant speed

The obvious way to handle an interruption is to simply begin a new path from the current position to the new target. With this approach, the output always moves towards the target at a constant hyperbolic speed. Specifically, for each change of target, follow the path $\text{geo}(\mathbf{y}_0, \mathbf{x}_1, ct)$, where \mathbf{y}_0 is the current output at the time of the target change, \mathbf{x}_1 is the new target, c is the speed of the animation, and t is the time elapsed since the target change. When $ct \geq \text{dist}(\mathbf{y}_0, \mathbf{x}_1)$, the target has been reached, and so the output should remain at the target until the next change of target.

The problem with this technique is that every time the target is reached, and every time the target is changed⁴, a velocity discontinuity is introduced into the smoothed signal. These discontinuities are easily seen in a world/screen diagram, as illustrated in Figure 8a.

7.2 Easing curves

Another simple solution is to use an *easing curve*. As we will show, this solves the problem of velocity discontinuities at the endpoints, but does not solve the problem of interruptions.

The easing curve can be specified as follows: for each change of target, follow the path $\text{gerp}(\mathbf{y}_0, \mathbf{x}_1, f(t/d))$, where \mathbf{y}_0 is the current output at the time of the target change, \mathbf{x}_1 is the new target, d is the desired duration of the animation, t is the elapsed time since the target change, and f is an *easing curve*, which satisfies $f(0) = 0$ and $f(\alpha) = 1$ for all $\alpha \geq 1$. The easing curve should also satisfy $f'(0) = f'(1) = 0$, where f' denotes the derivative of f . One easing curve that satisfies these properties is

$$f(\alpha) = \begin{cases} (1/2) - (1/2) \cos(\pi\alpha) & \alpha < 1 \\ 1 & \alpha \geq 1 \end{cases}$$

but there are many other options as well.

Provided that $f'(0) = f'(1) = 0$, this approach does not suffer from velocity discontinuities at the endpoints. However, it does not handle the case of interruptions, since an interruption would cause the velocity to abruptly jump to zero as the new animation segment begins. The velocity discontinuities introduced by interruptions in the easing approach are easily seen in the world/screen diagram, as shown in Figure 8b.

One difference between this technique and the previous technique is that the duration of the animations produced using this technique is fixed, whereas for the previous technique, the duration of the animations produced is proportional to the distance between the start point and the target point. We do not claim that having a fixed duration is superior to a variable duration or vice versa—the choice depends on the specific effect the interaction designer is trying to achieve.

⁴Except, of course, for the edge case where the new target happens to lie on the same geodesic as the current target, and in the same direction.

8 SMOOTHING USING GEODESIC ONE-POLE FILTERS

To solve the problem of smoothing both the endpoints and interruptions, we introduce a novel technique for smooth and efficient zooming and panning that draws inspiration from signal processing. While signal processing techniques have previously been used to animate Euclidean attributes [17], to process orientation signals [13], and to process signals on a sphere [15], to our knowledge signal-processing techniques have not been applied to signals in hyperbolic space.

The techniques of the previous section were formulated in terms of target changes, and each target change triggered a change in the formulation of the output. In this section, we take a different approach. Instead of processing target change events, we instead process the target signal directly, transforming the target signal into the smoothed signal using differential equations. There are many ways to perform this transformation, and different methods will produce different animations. This section introduces a particularly simple method, which is based on the *one-pole low-pass filter*, a common filter in signal processing. We call our technique the *geodesic one-pole filter*.

For the target signal $\mathbf{x}(t)$, the output $\mathbf{y}(t)$ of the geodesic one-pole filter is defined by the differential equation

$$\frac{d}{dt} \mathbf{y}(t) = \alpha \text{Log}_{\mathbf{y}(t)} \mathbf{x}(t) \quad (10)$$

where α controls the speed of the animation. This equation is depicted in block diagram form in Figure 9. This differential equation can be explained as follows: at every instant, walk along a geodesic towards the target with hyperbolic speed proportional to the hyperbolic distance to the target. This system is clearly causal, since the derivative of the output depends only on the current output and input. The output of this system is shown in Figure 10a.

8.1 Cascading filters

While the one pole filter does smooth its input, it is not strong enough for our purposes. As can be seen from (10), the derivative of the output is proportional to the difference between the input and the output. Because the output's derivative is always defined, the output will be continuous even if the input is not. However, it is clear from the definition that a discontinuity in the input will introduce a velocity discontinuity in the output.

To create a more powerful filter, we can cascade multiple instances of the one pole filter, i.e. place them in series. An example of this is shown in Figure 11. The output of the cascaded one-pole filter is shown in Figure 8c. Each additional one-pole filter used in a cascaded arrangement increases the order of smoothness. A single one-pole filter produces an output with continuous position. Cascading two one-pole filters produces an output with continuous velocity. Cascading three one-pole filters produces an output with continuous acceleration. Cascading four one-pole filters produces an output with continuous jerk.

8.2 Limiting the hyperbolic speed

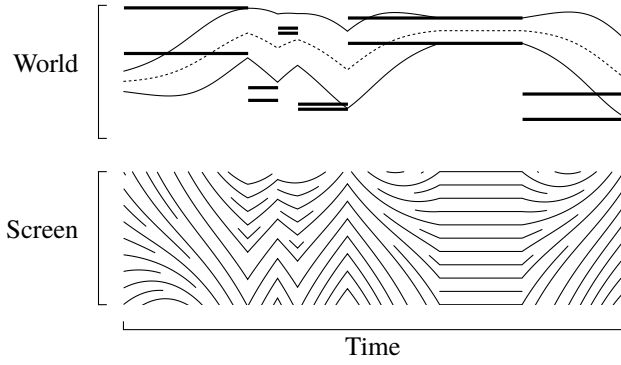
Like the easing curve method, the one-pole filter will produce animations where the hyperbolic speed is greater for far-away targets than for nearby targets. For some use-cases, this can be undesirable, and so we will now discuss a simple modification of the one-pole filter that limits the maximum speed of the animation.

To accomplish this, we first define the function $\text{clipvec}(\mathbf{X}, c)$ as follows:

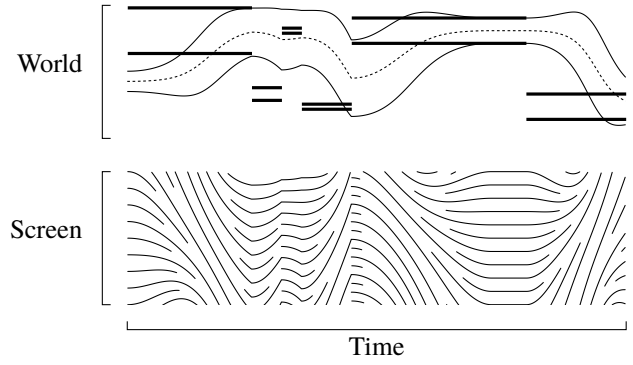
$$\text{clipvec}(\mathbf{X}, c) = \begin{cases} \mathbf{X} & |\mathbf{X}| < c \\ c \frac{\mathbf{X}}{|\mathbf{X}|} & |\mathbf{X}| \geq c \end{cases} \quad (11)$$

This function takes a vector $\mathbf{X} \in \mathbb{T}_x \mathbb{H}^n$ and modifies its magnitude hyperbolic $|\mathbf{X}|$ so that it does not exceed a threshold c . Using this function, we can then define the clipped geodesic one-pole filter as

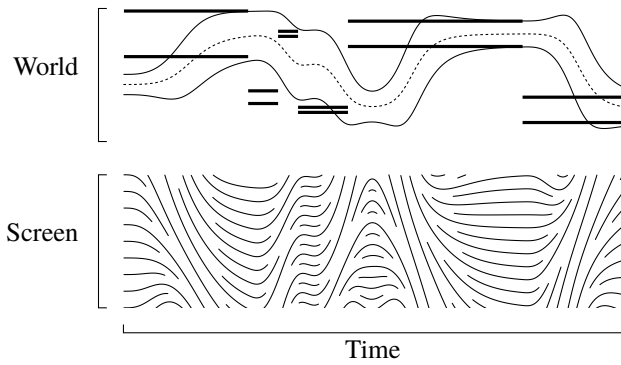
$$\frac{d}{dt} \mathbf{y}(t) = \text{clipvec}\left(\alpha \text{Log}_{\mathbf{y}(t)} \mathbf{x}(t), c\right) \quad (12)$$



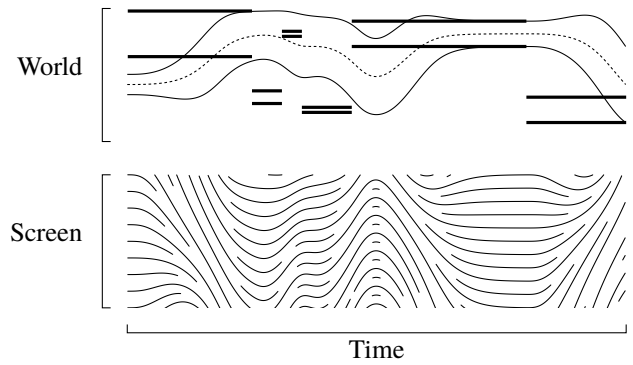
(a) Constant speed



(b) Easing curve



(c) Cascaded one-pole filter



(d) Clipped cascaded one-pole filter

Fig. 8: These world/screen diagrams depict the result of different zooming and panning approaches applied to the same target signal. In these diagrams the target signal is depicted as a pair of bold lines that shows the desired world span. The constant-speed technique uses the optimal navigation approach of van Wijk and Nuij [18] to produce an animation towards the current target. The easing curve technique shows a straightforward modification of optimal navigation. As can be seen, neither the constant-speed technique (a) nor the easing curve technique (b) are smooth when interrupted. For both of these techniques, interruptions produce velocity discontinuities in screen space. By contrast, a geodesic one-pole filter cascaded four times (c) is smooth even when interrupted, as is the clipped cascaded one-pole filter (d).

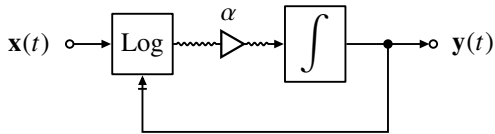


Fig. 9: The geodesic one-pole filter, given by (10), can be depicted as a block diagram. Each wire in this diagram represents a signal: solid wires represent signals whose values are hyperbolic points, and wavy wires represent signals whose values are hyperbolic vectors. The triangular element represents multiplication. The integral block represents the following relationship: the input to the block is the derivative of the block's output. The arrow with a bar pointing to Log denotes the subscript argument.

where c is a threshold that sets the maximum allowed hyperbolic speed. The output of this system is shown in Figure 10b. By placing in series a clipped one-pole filter followed by three geodesic one-pole filters, a system is formed whose output is smooth and whose speed is limited. We call this system the *clipped cascaded geodesic one-pole filter*. The video demo that accompanies this paper uses the values $c = 1$ Hz for the first filter and $\alpha = 6$ Hz for all four filters⁵.

8.3 Discretizing the one-pole filter

The previous section described solutions to the interruptible zooming and panning problem in terms of cascaded first-order differential equations. To write a program that implements one of these solutions, any ordinary differential equation (ODE) solver can be used to numerically approximate these differential equations. In this section, however, we take an alternative approach: we convert the continuous-time systems described in the last section into discrete-time systems. The solution we arrive at is quite simple, and does not require the use of an external ODE solver.

Notice that the geodesic one-pole filter (10) and the clipped geodesic

⁵These definitions of c and α assume that distance in hyperbolic space is unitless, as is the case when the metric is unitless. If the metric were defined strictly as the root-mean-square velocity of the optical flow on a physical screen, then c would instead have units of speed (meters per second). However, in this case, the value of c would depend on the size of the screen.

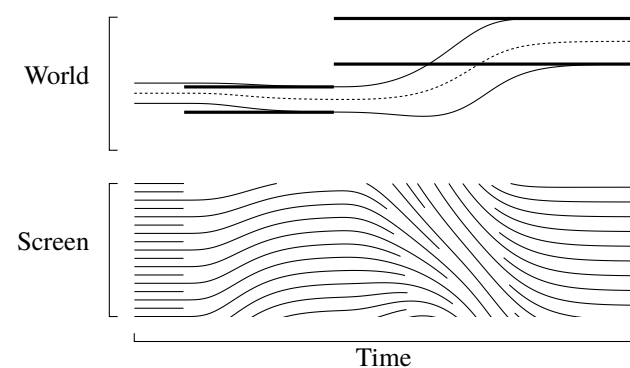
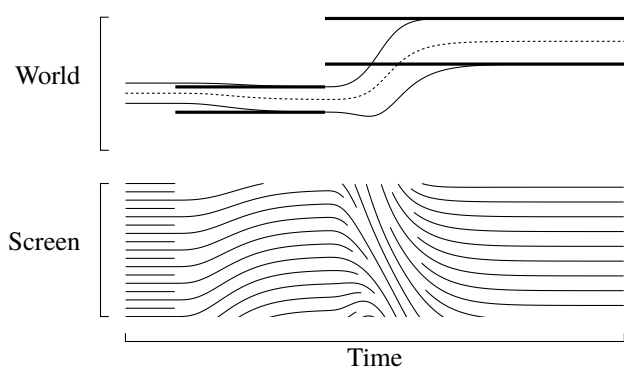
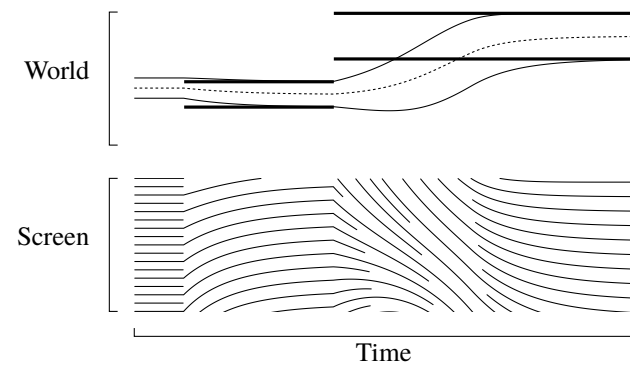
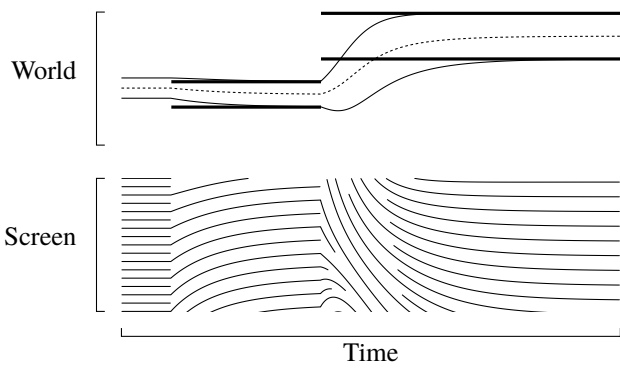


Fig. 10: The geodesic one-pole filter (a) produces faster zooming and panning animations for targets that are farther away. The clipped one-pole filter (b), by contrast, limits the maximum speed of the animation. For discontinuous input, neither of these systems produces smooth zooming and panning animations, but they can be combined with additional one-pole filters to produce smoother animations, as shown in (c) and (d).

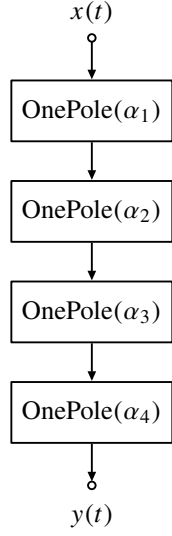


Fig. 11: The output of a single one-pole filter is continuous in position, but may not be continuous in velocity. In order to guarantee that the output is smooth to a higher degree, one-pole filters can be chained together. The filter depicted in this diagram, in which four one-pole filters are cascaded, produces an output with continuous position, velocity, acceleration, and jerk. Each block $\text{OnePole}(\alpha)$ denotes the filter structure shown in Figure 9.

one-pole filter (12) have the form

$$\frac{d}{dt} \mathbf{y}(t) = f(\mathbf{y}(t), \mathbf{x}(t)) \quad (13)$$

where $f(\mathbf{y}(t), \mathbf{x}(t)) \in \mathbb{T}_{\mathbf{y}(t)}$. A differential equation of this form can be approximated by

$$\mathbf{y}[i] = \text{Exp}(Tf(\mathbf{y}[i-1], \mathbf{x}[i])) \quad (14)$$

where T is the sampling period and $f(\mathbf{y}[i-1], \mathbf{x}[i]) \in \mathbb{T}_{\mathbf{y}[i-1]}$. To see that this does approximate the continuous-time system, note that (14) can be written as

$$\mathbf{y}(t) = \text{Exp}(Tf(\mathbf{y}(t-T), \mathbf{x}(t))).$$

Taking the logarithmic map of both sides with base $\mathbf{y}(t-T)$ and then dividing both sides by T gives

$$\frac{\text{Log}_{\mathbf{y}(t-T)} \mathbf{y}(t)}{T} = f(\mathbf{y}(t-T), \mathbf{x}(t))$$

Taking the limit as T goes to zero gives (13).

Applying this approximation to the geodesic one-pole filter (10) and simplifying using (7) gives

$$\mathbf{y}[i] = \text{gerp}(\mathbf{y}[i-1], \mathbf{x}[i], b) \quad (15)$$

where $b = \alpha T$ for sampling period T . In other words, at each frame, we take step towards the target, where the length of the step is proportional to the distance to the target. A block diagram of this approximation is shown in Figure 12. Note that this approximation oscillates for $b > 1$ and is unstable for $b > 2$, and so the sampling period T should be small enough that $b < 1$.

To approximate the cascaded one-pole system shown in Figure 11, we can simply cascade the discrete one-pole filters as shown in Figure 13.

Applying the approximation given by Equations (13) and (14) to the clipped one-pole filter (12) and simplifying gives

$$\mathbf{y}[i] = \text{geo}(\mathbf{y}[i-1], \mathbf{x}[i], s[i]) \quad (16a)$$

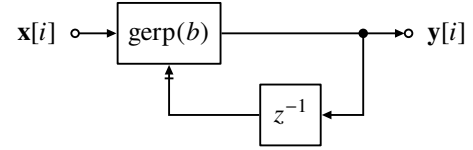


Fig. 12: The discrete-time hyperbolic one-pole filter is an approximation to the continuous-time one-pole filter depicted in Figure 9. The element z^{-1} denotes a delay by one sample, i.e. a delay by the sampling period T . The block $\text{gerp}(b)$ denotes $\text{gerp}(\mathbf{x}_0, \mathbf{x}_1, b)$, where the arrowhead with a bar in the diagram corresponds to \mathbf{x}_0 and the arrowhead without a bar in the diagram corresponds to \mathbf{x}_1 .

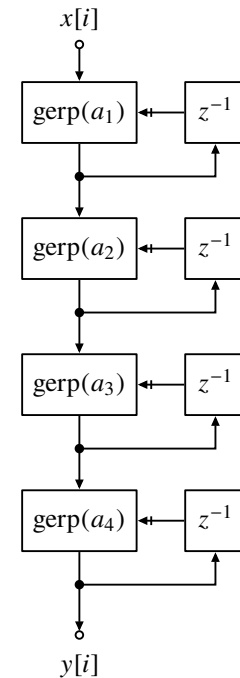


Fig. 13: The cascaded one-pole system depicted in Figure 11 can be discretized by cascading the discrete one-one pole blocks depicted in Figure 12.

$$s[i] = T \min(c, \alpha S[i]) \quad (16b)$$

$$S[i] = \text{dist}(\mathbf{y}[i-1], \mathbf{x}[i]) \quad (16c)$$

where T is the sampling period.

9 SMOOTHING USING GEODESIC TWO-POLE FILTERS

The technique discussed in the previous section formed higher-order filters by cascading one-pole filters. Animations that make use of these filters travel directly to their target, settling in slowly. Suppose that we instead wanted an animation where the camera overshoots the target slightly before settling in a spring-like motion. To achieve this effect, we can use a two pole filter, which models the behavior of a spring-mass-damper system.

In Euclidean space, a spring-mass-damper system experiences two forces: a spring force that pulls the mass towards the equilibrium position and is proportional to the displacement from this equilibrium position, and a damping force that pushes against the mass's velocity. The spring-mass-damper system can be adapted to hyperbolic space as

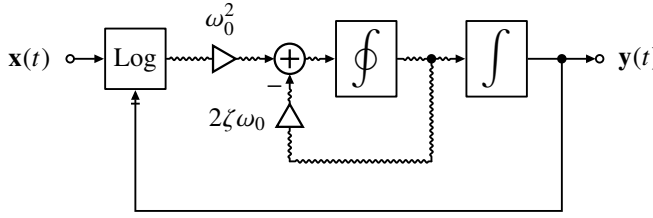


Fig. 14: The geodesic two-pole filter defined by (17) can be depicted as a block diagram. Here, the integral with a circle represents the following relationship: the input to the block is the covariant derivative of the output.

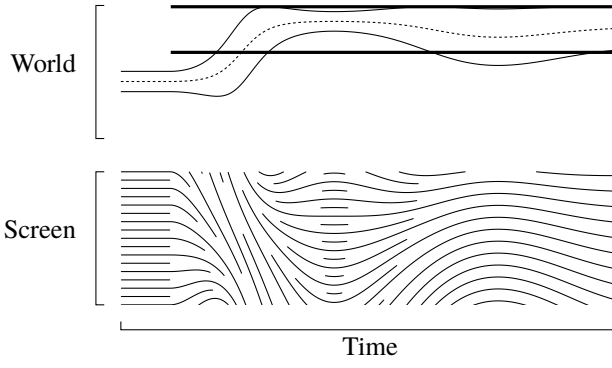


Fig. 15: The geodesic two-pole filter defined by (17) produces spring-like motion.

follows:

$$\frac{D}{dt} \frac{d}{dt} \mathbf{y}(t) = \omega_0^2 \text{Log}_{\mathbf{y}(t)}(\mathbf{x}(t)) - 2\zeta\omega_0 \frac{d}{dt} \mathbf{y}(t) \quad (17)$$

The variable ω_0 controls the rate of the animation, and the parameter ζ controls the damping. When $\zeta < 1$, the system oscillates in a spring-like motion as it settles. A block diagram of this is shown in Figure 14. The response of the two-pole filter for discontinuous input is shown in Figure 15.

The system defined by (17) can of course be placed in series with a one-pole filter or another two-pole filter. Like the one-pole filter and easing curves, animation produced by the two-pole filter will be faster for distant targets than for nearby targets. A simple way to address this is to place the clipped one-pole filter in series with the two-pole filter. We call the system consisting of a single clipped one-pole filter followed by a two-pole filter the *clipped geodesic two-pole filter*. Another way to reduce the speed for distant targets would be to use quadratic damping instead of linear damping, but this paper does not explore this option.

9.1 Discretizing the two-pole filter

As with the continuous-time one-pole filter, the differential equation given by (17) can be approximated using a standard ODE solver. However, we can also write a simple approximation by converting the continuous-time system to a discrete-time system.

Notice that the geodesic two pole filter has the form

$$\frac{D}{dt} \frac{d}{dt} \mathbf{y}(t) = f(\mathbf{y}(t), \mathbf{y}(t), \mathbf{x}(t)) \quad (18)$$

where $\mathbf{y}(t)$ denotes the time derivative of $\mathbf{y}(t)$. A system of this form can be approximated by

$$\mathbf{y}[i] = \mathbf{y}[i-1] + T f(\mathbf{y}[i-1], \mathcal{T}_{\mathbf{y}[i-1]} \mathbf{y}[i-1], \mathbf{x}[i]) \quad (19)$$

$$\mathbf{y}[i] = \text{Exp}(T \mathbf{y}[i]) \quad (20)$$

Here both $\mathbf{y}[i] \in \mathbb{H}^n$ and $\mathbf{y}[i] \in \mathbb{T}_{\mathbf{y}[i-1]} \mathbb{H}^n$ are state variables that are updated at each frame. The parallel transport in this formula is necessary to move the vector variable $\mathbf{y}[i]$ to the correct location each time the position variable $\mathbf{y}[i]$ is updated.

Applying this approximation to the geodesic two-pole filter gives

$$\mathbf{y}[i] = (1 - 2T\zeta\omega_0) \mathcal{T}_{\mathbf{y}[i-1]}(\mathbf{y}[i-1]) \quad (21)$$

$$+ T\omega_0^2 \text{Log}_{\mathbf{y}[i-1]}(\mathbf{x}[i])$$

$$\mathbf{y}[i] = \text{Exp}(T \mathbf{y}[i]). \quad (22)$$

The demo videos that accompany this paper have sixty frames per second, and so $T = (1/60)$ s.

10 CONCLUSION AND FUTURE WORK

We have introduced the hyperbolic model of zooming and panning. This model exploits the Poincaré half-space model of hyperbolic space to model zooming and panning. Using this model, we have introduced novel zooming and panning animation techniques based on signal processing and Riemannian geometry. These animation techniques produce smooth zooming and panning animations to a target value, and these animations remain smooth even when the animation is interrupted by a change of target. Such interruptions are common in interactive uses, where user input can interrupt zooming and panning animations at any time.

We have also introduced world/screen diagrams to visualize zooming and panning animations. These diagrams emphasize the perceptual aspects of zooming and panning, and are useful for evaluating different zooming and panning techniques.

There are many avenues for future work. For example, if instead of the interactive zooming and panning problem we have investigated in this paper, we merely wish to interpolate a set of target points, the Bézier curve generalization of Park and Ravani [16] can be straightforwardly applied to zooming and panning using the definitions we presented here. The animation model in this paper could also be applied to other navigation problems, e.g. lenses [1, 3] or zooming and panning on a globe. Finally, there are possible variations on the specific signal processing systems we have introduced that could be explored in future work.

This paper has used the Poincaré half-space model to represent zooming and panning positions. However, there are many other possible coordinate systems that could be used for hyperbolic space. While the results remain the same regardless of coordinate system, different coordinate systems might be more convenient for particular purposes. Other well-known representations for hyperbolic space include the Poincaré disk model, the Klein model, and the hyperboloid model [4]. Another option would be to use space-scale diagrams. Yet another option would be to a model in which the altitude of the camera is constant and the angle of view is varied to zoom and pan. Such a model would match the term “zooming” more closely, since zooming on a camera involves changing the angle of view rather than changing the position of the camera.⁶

11 ACKNOWLEDGMENTS

This research was supported in part by NSF grant IIS-1447416.

REFERENCES

- [1] C. Appert, O. Chapuis, and E. Pietriga. High-precision magnification lenses. In *Proceedings of the SIGCHI Conference on Human Factors in Computing Systems*, pages 273–282. ACM, 2010.
- [2] B. B. Bederson, J. Meyer, and L. Good. Jazz: an extensible zoomable user interface graphics toolkit in java. In *Proceedings of the 13th annual ACM symposium on User interface software and technology*, pages 171–180. ACM, 2000.

⁶In fact, it might be more accurate to refer to the model used in this paper as dollying and panning rather than zooming and panning.

- [3] E. A. Bier, M. C. Stone, K. Pier, W. Buxton, and T. D. DeRose. Tool-glass and magic lenses: the see-through interface. In *Proceedings of the 20th annual conference on Computer graphics and interactive techniques*, pages 73–80. ACM, 1993.
- [4] J. W. Cannon, W. J. Floyd, R. Kenyon, W. R. Parry, et al. Hyperbolic geometry. *Flavors of geometry*, 31:59–115, 1997.
- [5] A. Cockburn, A. K. Karlson, and B. B. Bederson. A review of overview+ detail, zooming, and focus+ context interfaces. *ACM Comput. Surv.*, 41(1):2–1, 2008.
- [6] M. P. Do Carmo and J. Flaherty Francis. *Riemannian geometry*, volume 115. Birkhäuser Boston, 1992.
- [7] P. Dragicevic, A. Bezerianos, W. Javed, N. Elmquist, and J.-D. Fekete. Temporal distortion for animated transitions. In *Proceedings of the SIGCHI Conference on Human Factors in Computing Systems*, pages 2009–2018. ACM, 2011.
- [8] G. W. Furnas and B. B. Bederson. Space-scale diagrams: Understanding multiscale interfaces. In *Proceedings of the SIGCHI conference on Human factors in computing systems*, pages 234–241. ACM Press/Addison-Wesley Publishing Co., 1995.
- [9] Y. Guiard, M. Beaudouin-Lafon, J. Bastin, D. Pasveer, and S. Zhai. View size and pointing difficulty in multi-scale navigation. In *Proceedings of the working conference on Advanced visual interfaces*, pages 117–124. ACM, 2004.
- [10] T. Igarashi and K. Hinckley. Speed-dependent automatic zooming for browsing large documents. In *Proceedings of the 13th annual ACM symposium on User interface software and technology*, pages 139–148. ACM, 2000.
- [11] J. Lee. *Riemannian manifolds : an introduction to curvature*. Springer, New York, 1997.
- [12] J. Lee. *Introduction to smooth manifolds*. Springer, New York London, 2012.
- [13] J. Lee and S. Y. Shin. General construction of time-domain filters for orientation data. *Visualization and Computer Graphics, IEEE Transactions on*, 8(2):119–128, 2002.
- [14] V. Matvienko and J. Krüger. Dense isocontour imaging. In *SIGGRAPH Asia 2013 Technical Briefs*, page 16. ACM, 2013.
- [15] J. M. Osborne and G. P. Hicks. The geodesic spring on the euclidean sphere with parallel-transport-based damping. *Notices of the American Mathematical Society*, 60(5):544–557, 2013.
- [16] B. Ravani and F. C. Park. Bézier curves on riemannian manifolds and lie groups with kinematics applications. 1995.
- [17] A. M. Reach and C. North. The signals and systems approach to animation, 2017.
- [18] J. J. van Wijk and W. A. Nuij. Smooth and efficient zooming and panning. In *Information Visualization, 2003. INFOVIS 2003. IEEE Symposium on*, pages 15–23. IEEE, 2003.
- [19] J. J. Van Wijk and W. A. Nuij. A model for smooth viewing and navigation of large 2D information spaces. *IEEE Transactions on Visualization and Computer Graphics*, 10(4):447–458, 2004.